Customized Stent-Grafts for Endovascular Aneurysm Repair with Challenging Necks: a Numerical Proof of Concept

André Hemmler[1] | Andrew Lin[2] | Nikolaus Thierfelder[3] | Thomas Franz[4] | Michael W. Gee[1] | Deon Bezuidenhout[2]

[1]Mechanics & High Performance Computing Group, Technische Universität München, 85748 Garching b. München, Germany

[2]Chris Barnard Division of Cardiothoracic Surgery, University of Cape Town, 7925 Observatory, South Africa

[3]Herzchirurgische Klinik und Poliklinik, Ludwig-Maximilians-Universität München, 81377 München, Germany

[4]Division of Biomedical Engineering, Department of Human Biology, University of Cape Town, 7925 Observatory, South Africa

Correspondence
Michael W. Gee, Mechanics & High Performance Computing Group, Technische Universität München, 85748 Garching b. München, Germany. Email: gee@tum.de

Summary

Endovascular aortic repair (EVAR) is a challenging intervention whose long-term success strongly depends on the appropriate stent-graft (SG) selection and sizing. Most off-the-shelf SGs are straight and cylindrical. Especially in challenging vessel morphologies, the morphology of off-the-shelf SGs is not able to meet the patient-specific demands. Advanced manufacturing technologies facilitate the development of highly customized SGs. Customized SGs that have the same morphology as the luminal vessel surface could considerably improve the quality of the EVAR outcome with reduced likelihoods of EVAR related complications such as endoleaks type I and SG migration.

In this contribution, we use an in silico EVAR methodology that approximates the deployed state of the elastically deformable SG in a hyperelastic, anisotropic vessel. The in silico EVAR results of off-the-shelf SGs and customized SGs are compared qualitatively and quantitatively in terms of mechanical and geometrical parameters such as stent stresses, contact tractions, SG fixation forces and the SG-vessel attachment. In a numerical proof of concept, eight different vessel morphologies, such as a conical vessel, a barrel shaped vessel and a curved vessel, are used to demonstrate the added value of customized SGs compared to off-the-shelf SGs.

The numerical investigation has shown large benefits of the highly customized SGs compared to off-the-shelf SGs with respect to a better SG-vessel attachment and a considerable increase in SG fixation forces of up to 50% which indicate decreased likelihoods of EVAR related complications. Hence, this numerical proof of concept motivates further research and development of highly customized SGs for the use in challenging vessel morphologies.

KEYWORDS:
abdominal aortic aneurysm, endovascular repair, customized stent-graft, personalized medicine

1 | INTRODUCTION

An aortic aneurysm is an abnormal dilatation of the aorta that is mostly asymptomatic. Endovascular aortic repair (EVAR) involves the deployment of a stent-graft (SG) inside the aneurysm to exclude the aneurysm sac from the main blood flow and

prevent the aneurysm from rupture. Most SGs are composed of metallic stents that are attached to a polymeric fabric (graft). In clinical practice, SGs are cylindrical off-the-shelf devices. This means in the preinterventional planning length and diameter of the SG are determined based on preinterventional CT data, but the patient-specific vessel morphology is not considered. EVAR requires a proper seal and fixation of the SG in the SG landing zones, i.e. in the regions proximal and distal of the aneurysm, to keep the aneurysm permanently excluded from the main blood flow. However, especially in the case of challenging aneurysm neck morphologies, i.e. challenging vessel morphologies in the region of the proximal landing zone, the morphological discrepancy between the cylindrical off-the-shelf SG and the vessel might lead to negative effects and possible secondary interventions[62,49]. Frequent negative effects after EVAR that are directly related to the conditions in the SG landing zone are, among others, type I endoleaks[17,6] and SG migration[54,50,1]. Most frequently mentioned challenging neck morphologies are highly angulated and short necks[25,48,60]. But also conically shaped, barrel shaped, hourglass shaped or elliptic necks are frequently associated with negative effects in the SG landing zones[31,58] since these nonuniform neck morphologies lead to nonuniform SG expansion, reduced seal and reduced fixation of the SG.

Most of the existing SGs are of cylindrical shape that are unable to meet the vessel morphology of different patients. Nonuniform vessel morphologies require customized SG morphologies. This raises the need of a more personalized therapy where customized SGs[44,49,62] can be the next generation SGs for EVAR. By considering the vessel morphology in the region of the landing zone, the SG performance and the SG-vessel interaction should be improved leading to better long-term EVAR outcomes and a reduced number of EVAR related complications and secondary interventions. Currently, the usage of EVAR is limited to friendly necks as stated in the instructions for use (IFU) of the device manufacturers, such as neck angles below 60° and necks with a limited degree of conical shape[34,58]. Besides reduced complication rates after EVAR in challenging necks, customized SGs could further increase the range of applicability of EVAR far beyond the IFUs of current SG manufacturers. Advanced manufacturing technologies like additive manufacturing or electrospinning have proved to be able to meet the demands of personalized medicine in wide ranges of medical applications[43,38]. However, the use of these advanced manufacturing technologies in the development of highly customized SGs for EVAR is still current area of research[62] and the benefit of highly customized SGs over off-the-shelf SGs could not yet be proved. To qualitatively and quantitatively show the benefit of customized SGs compared to off-the-shelf SGs, in silico EVAR approaches[21,39,2] are a valuable tool. Further, numerical investigations can provide information on specific SG design aspects for advanced development of highly customized SGs.

The objective of this study is to show the added value of customized SGs that have the same morphology as the luminal vessel surface in a numerical proof of concept by using the in silico EVAR methodology proposed in[20]. This in silico EVAR methodology approximates the final state of the deployed SG after intervention. By comparison of the in silico EVAR outcome of off-the-shelf SGs and customized SGs, the performance differences of the two SG types is assessed in terms of mechanical and geometrical parameters such as stent stresses, contact tractions, SG fixation forces and the SG-vessel attachment. The focus of these mechanical and geometrical parameters is on parameters which define the quality of the EVAR outcome in the landing zone of the SG and which indicate the potential complication likelihood after EVAR.

In order to represent different aspects of noncylindrical geometries encountered in patient-specific anatomies, in this study general vessel morphologies, such as curved, conical, barrel shaped or hourglass shaped vessel morphologies are used in a numerical proof of concept. Although idealized vessels are studied, we consider a realistic state of the deployed SG which takes stent predeformation[20], vessel prestressing[15] and physiological blood pressure states into account. The applied methods are shown for the abdominal region of the aorta. Nevertheless, the results are also applicable to endovascular repair of other regions of the aorta such as thoracic endovascular aortic repair. Further, the presented approach of customized stent-grafts for standard EVAR is transfarable without restrictions to fenestrated prostheses for application in juxtarenal AAAs or infrarenal AAAs with challenging proximal neck anatomy.

Common medical practice is the customization of fenestrated SGs[55,36] where the location of the fenestration is done in a patient-specific manner. Apart from this type of SG customization of advanced EVAR techniques, we propose the classification of customized SGs into two different levels of customization (Figure 1). The first level of SG customization describes an individual arrangement of stent rings on a classical graft to better meet the requirements of a patient-specific vessel. However, similar to off-the-shelf SGs the morphology of first level customized SGs is cylindrical and straight in the undeformed state. Romarowski et al.[44] numerically showed the advantage of such first level customized SGs compared to two off-the-shelf SGs.

In contrast to first level customized SGs, second level customized SGs are not cylindrical and straight, but are of the same morphology as the patient-specific luminal vessel surface and hence can even better meet the requirements of patient-specific vessels. To the best of the authors knowledge, the work by Zhang et al.[62] is the only published study on second level customized
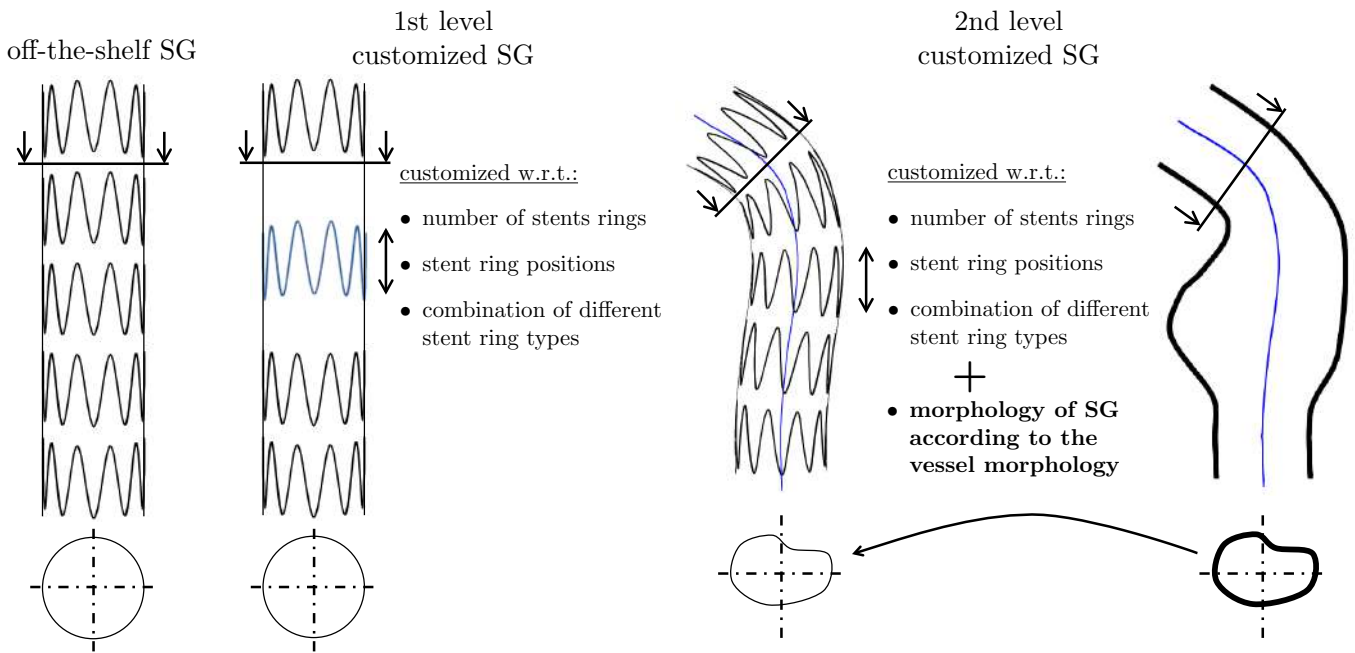
FIGURE 1 Sketch of a straight, cylindrical off-the-shelf SG as well as a first level and a second level customized SG.

SGs. Zhang et al.[62] proposed a manufacturing technique of customized SGs which have the same morphology as the patient-specific vessel but did not investigate the advantage of this type of customized SGs compared to off-the-shelf SGs.

The outline of this paper is as follows: in section 2, the morphological advantages of second level customized SGs are investigated theoretically. Afterwards, we describe the basic concept of the manufacturing process of the presented customized SGs. Further, we present the models of off-the-shelf SGs, customized SGs as well as the vessel, give an overview of the in silico EVAR methodology and describe the framework of the presented numerical proof of concept. In section 3, we compare the in silico EVAR outcome of customized SGs to off-the-shelf SGs for several different vessel morphologies. The discussion of these results is presented in section 4. Subsequently, limitations and conclusions are drawn in section 5 and 6, respectively.

2 | MATERIALS AND METHODS

2.1 | Morphology of second level customized stent-grafts

The regions proximal and distal of the aneurysm, denoted as landing zones, have the greatest influence on the quality of the EVAR outcome[53,31]. Straight and cylindrical off-the-shelf SGs are not able to fully meet the requirements of angulated and nonuniform vessel morphologies in the region of the landing zone.

The degree of SG oversizing is a major design variable of SGs[54,5,47,50]. The degree of SG oversizing is given by

$$o = \frac{D^{\mathrm{SG}}}{D^{\mathrm{Ao}}} - 1, \tag{1}$$

where D^{SG} is the diameter of the SG and D^{Ao} is the preinterventional luminal diameter of the vessel at the region of the landing zone.

Given a noncylindrical vessel landing zone (e.g. a conical vessel landing zone (Figure 2I)), correct sizing of cylindrical off-the-shelf SGs is very challenging. Mostly, the maximum vessel diameter $D^{\mathrm{Ao}}_{\max}$ along the total potential vessel landing zone is chosen as recommended for instance in the IFU of Cook Zenith® SGs[8]. However, sizing of the SG according to the maximum vessel diameter $D^{\mathrm{Ao}}_{\max}$ results in excessive oversizing at narrow regions of the noncylindrical vessel ($o = o_{\max}$) which might result in long-term negative effects such as aortic neck dilatation[54,57]. Using the minimum vessel diameter $D^{\mathrm{Ao}}_{\min}$ for sizing of the cylindrical off-the-shelf SGs increases the risk of SG undersizing at wide regions of the noncylindrical vessel ($o = o_{\min}$) with its negative consequences such as endoleaks type I. Using second level customized SGs that have the same morphology as the
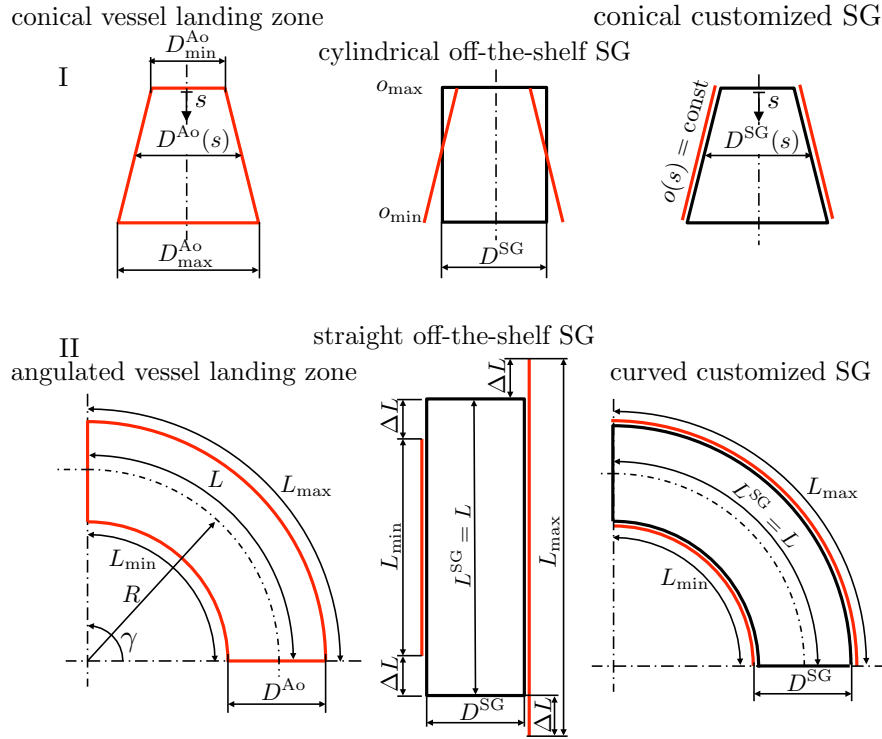
FIGURE 2 Illustration of SG sizing problems of off-the-shelf SGs in a conical vessel landing zone (I) and an angulated vessel landing zone (II) as well as improvement by second level customized SGs. Vessel landing zones are visualized in red, SGs in black.

vessel, this inconsistency in SG sizing is obsolete. A constant degree of SG oversizing ($o(s) = $ const) along the total arc length s of the vessel can be achieved (Figure 2I).

The length of the landing zone is one of the most important parameters for positive EVAR outcomes[53,32]. Hence, the length of the SG generally is chosen such that all of the potential length of the vessel landing zone is used, i.e. is covered by the SG. Given an angulated vessel landing zone (Figure 2II), the effective length of the landing zone is smaller at the inner curvature of the vessel ($L_{\min} = \frac{\gamma}{180}\pi(R - \frac{D^{\mathrm{Ao}}}{2})$) than at the outer curvature of the vessel ($L_{\max} = \frac{\gamma}{180}\pi(R + \frac{D^{\mathrm{Ao}}}{2})$)[53]. Generally, the vessel centerline is used to determine the SG length. A straight off-the-shelf SG of length $L^{\mathrm{SG}} = L$ is not able to use the total potential length of the vessel landing zone as it is too long at the inner curvature and too short at the outer curvature by $2\Delta L$ where ΔL is given by

$$\Delta L = L - L_{\min} = L_{\max} - L = \frac{\gamma}{180}\pi\frac{D^{\mathrm{Ao}}}{4}. \tag{2}$$

This means that a length of $2\Delta L$ of the potential vessel landing zone at the outer curvature of the vessel remains unused. Excess length of the SG at the inner curvature of the vessel has to be avoided as well. This leads to longitudinal buckling of the graft at the inner curvature with its associated negative effects on the EVAR outcome such as disturbance of the blood flow. Being able to use the total potential length of the vessel landing zone $L_{\max}$ at the outer curvature of the vessel while at the same time the SG is not too long at the inner curvature of the vessel can contribute positively to the sealing and fixation of the SG. Second level customized SGs which have the same angulation as the vessel landing zone can exploit much better the restricted length of the important vessel landing zone with different effective lengths at the inner and the outer curvature (Figure 2II).

2.2 | Basic manufacturing idea of second level customized stent-grafts

Even though the focus of the current paper is not on manufacturing of customized SGs and its technical feasibility, but rather on giving a motivation for further research and development of this kind of SGs, the basic concept of the presented customized SGs is given. Discussions of specific manufacturing details are not part of this study, but will be presented in a future study by our group.

In a first step using 3D printing, a mandrel according to the patient-specific vessel geometry from CT data is created. Using electrospinning, this customized conductive mandrel is covered by a polyurethane (PU) graft that encapsulates nitinol stent rings. After removal of the mandrel, a customized SG is obtained which in the undeformed state has the same shape as the patient-specific luminal vessel geometry.

Manufacturing of various geometries (conical, elliptical, curved and straight) to determine the limits of electrospinning showed very promising results. Initial experiments have shown that the described manufacturing process allows to manufacture complex geometry SGs with radial expansion forces similar to commercial prostheses.

Insertion and delivery of the customized stent grafts will be very similar to the procedures used for off-the-shelf ones in terms of delivery sheaths, ports and guide wires, due the highly conforming nature of the devices during crimping. Modifications for enhancement for accurate longitudinal and rotational positioning of the patient-specific (especially curved) geometries of the EVAR, as well as those facilitating sheathing and de-sheathing, are foreseen. These include steerable catheters for improved negotiation of tortuous aortic segments, enhancement of positioning markers for precise placement, and invaginating sections for the abrogation of shear forces during loading and delivery. Although these issues are not within the scope of the current paper, they are already investigation and form part of ongoing studies.

2.3 | Computational modeling

In the study, the focus is on the performance of customized and off-the-shelf SGs in the SG landing zones. Hence, idealized proximal neck geometries are considered whereas the aneurysm sac is not part of the model. A state-of-the-art anisotropic, hyperelastic two-fiber model with transversely isotropic fiber dispersion[14] is utilized for the elastically deformable aortic wall with a constant wall thickness of 1.5mm[42]. The vessel is embedded in spring boundary conditions with a spring stiffness of 2.0 kPa/mm[33] on the abluminal vessel wall boundary.

The SG is made up of a series of sinusoidally shaped nitinol stent rings attached to the graft. Although the material properties of marketed woven grafts and electrospun grafts are slightly different, we apply the same material model to commercial and customized SGs to guarantee a fair comparison. Only the benefit of the customized shape of the SG is subject of this study, independent of the slight differences in the material behavior of woven and electrospun grafts. Further, similar stent shapes with ten sinusoidally shaped periods, a stent height of 15 mm and a wire thickness of 0.4 mm as well as the same graft thickness of 0.08 mm are used for the model of the off-the-shelf SG and the customized SG. The attachment between stent and graft is modeled by mortar based mesh tying constraints[41]. Stent predeformation of 15% is assumed for all stent rings[20]. According to[40] nitinol almost fully remains in its austenitic phase in the deployed state of the SG. Hence, as long as the crimping of the SG inside its delivery sheath is not explicitly modeled, the material model of nitinol does not necessarily need to be able to model the phase transformation between the austenitic and the martensitic phase. Therefore to reduce complexity of the given problem in a reasonable range, the material behavior of nitinol is modeled by a purely hyperelastic model without phase transformation as proposed in[21] and material parameters corresponding to the austenitic phase of nitinol are used. The graft is modeled by an isotropic and hyperelastic material model with reduced bending stiffness as previously proposed[20,26]. A summary of the constitutive models and model parameters of the aortic wall, stent and graft are provided in Appendix A.

The deployed configuration of the elastically deformable SG in the elastically deformable vessel under a stationary blood pressure state of 130 mmHg is approximated using the in silico EVAR methodology presented in[20]. The in silico EVAR approach does not model the single intrainterventional steps itself but only aims at finding the final deployed SG configuration. The simulation process consists of two main steps. In a first step the SG is crimped, bent and moved by a tailor-made morphing algorithm to position the SG inside the vessel. Afterwards, the SG is deployed inside the vessel where it unfolds and makes contact with the luminal surface of the vascular model.

The proposed in silico EVAR methodology uses geometrically nonlinear finite element methods including frictional contact with a friction coefficient of $\mu = 0.4$[51,39] between SG and vessel. Linear hexahedral elements with F-bar-based element technology[11] are applied to the aortic wall with an edge length of 0.75 mm. The stent geometry is discretized by linear, hexahedral elements with enhanced assumed strain technology with adaptive mesh refinement in the curved parts of the stent rings. Hexahedral solid-shell elements with advanced antilocking technologies[56] with an element edge length of 0.4 mm are used for the graft discretization (Figure 3III). An implicit, quasi-stationary nonlinear solver with a semi-smooth Newton approach[16] is used to solve the given nonlinear boundary value problem. All simulations have been performed using an in-house nonlinear finite element code. Running the simulations required approximately 6 h per case on 28 cores (Intel Haswell nodes, SuperMUC, Leibniz Supercomputing Centre).
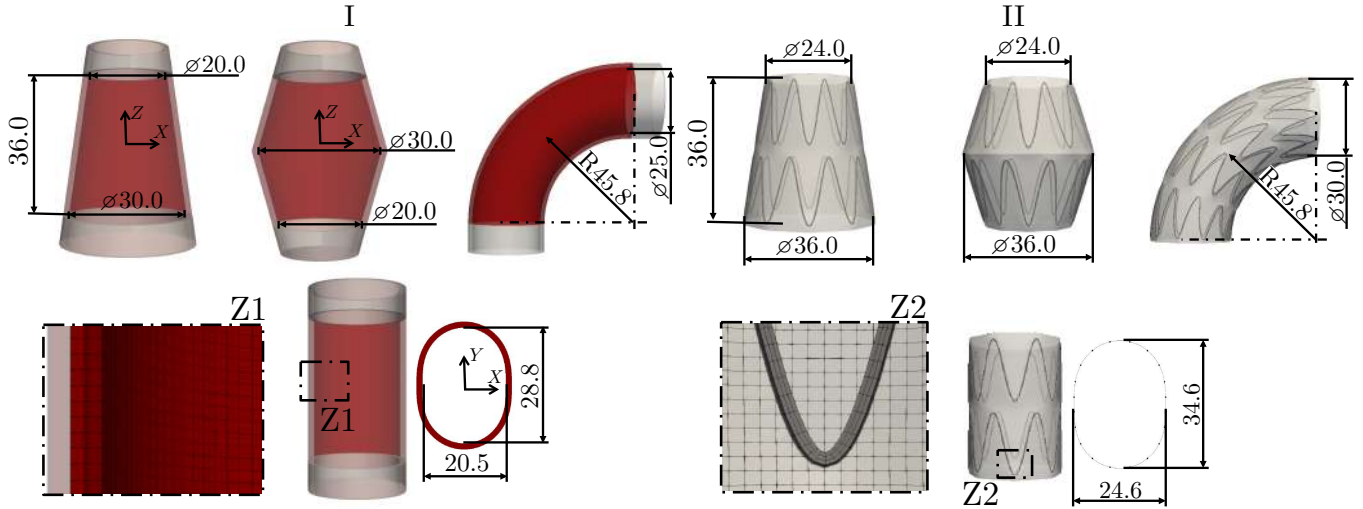
FIGURE 3 Exemplary depiction of vessel morphologies (I) and second level customized SGs (II). Discretization of the vessel (detail Z1) and SG model (detail Z2).

2.4 | Framework of the study

In a numerical proof of concept, we consider general vessel morphologies (Figure 3I) that are idealizations of realistic vessel shapes [31]. In [31], these vessel morphologies were defined to classify realistic patient-specific cases according to their shape in the proximal neck region. The objective of this study is to show the advantage of second level customized SGs (Figure 3II) that consider the morphology of the vessel compared to straight off-the-shelf SGs with a circular cross section.

A mean inner vessel diameter $\bar{D}^{\mathrm{Ao}} = 25$ mm is used for each of the consider vessel morphologies (Figure 3I). In case of the vessel with elliptical cross section, the quadratic mean diameter

$$\bar{D}^{\mathrm{Ao}} = \sqrt{\frac{a^2 + b^2}{2}} \tag{3}$$

is used where $a = 20.5$ mm is the length of the minor axis and $b = 28.8$ mm is the length of the major axis of the ellipse (Figure 3I).

A meaningful comparison between the cylindrical off-the-shelf SGs and the second level customized SGs is only possible if a similar degree of SG oversizing is used for both types of SGs. The cylindrical off-the-shelf SG has a constant diameter $\bar{D}^{\mathrm{Ao}} = 30$ mm which results in a variable degree of SG oversizing in the noncylindrical vessel. A mean SG oversizing $\bar{o} = 20\%$ is achieved by the constant SG diameter $\bar{D}^{\mathrm{Ao}} = 30$ mm in the noncylindrical vessels with a mean inner diameter $\bar{D}^{\mathrm{Ao}} = 25$ mm (equation (1)). The customized SGs, which have the same morphology as the vessel, are sized such that they have a constant degree of SG oversizing of $o = 20\%$. Hence, the local diameter of customized SGs is

$$D^{\mathrm{SG}}(s) = 1.2 D^{\mathrm{Ao}}(s), \tag{4}$$

where s is the arc length of the vessel centerline and $D^{\mathrm{Ao}}(s)$ is the local inner vessel diameter in an orthogonal plane to the vessel centerline at location s. The same SG length of 36 mm (72 mm for the curved SG) is used for the off-the-shelf and the customized SGs.

The consideration of curved vessels is of major importance as the IFU of SG manufacturers limit the application of EVAR mostly to neck angles below 60° since the likelihood of negative outcomes of off-the-shelf SGs is higher for larger neck angles. A vessel with an angle of $\gamma = 90°$ and a radius of curvature of $R = 45.8$ mm is chosen for the current study (Figure 3I). The radius of curvature of $R = 45.8$ mm is chosen such that the arc length of the centerline of the curved vessel is 72 mm. In keeping with the straight vessel examples, the curved vessel has a luminal diameter of 25 mm. In contrast to the considered SGs of the straight vessels, the SGs for the curved vessel consist of four stent rings (Figure 3II). All other SG related characteristics are equivalent to the examples of straight vessels.

In total, we consider seven different straight vessels (cylindrical, conical, elliptical, barrel shaped, hourglass shaped and two irregularly shaped vessels) as well as one curved vessel with a cylindrical cross section. For each of the eight different vessel
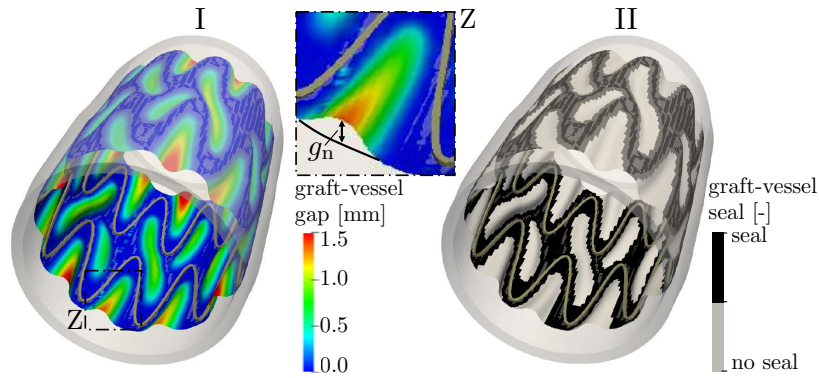
FIGURE 4 Exemplarily visualization of the graft-vessel gap (I) and the graft-vessel seal (II).

morphologies, we qualitatively and quantitatively compare the in silico EVAR outcome of the customized SG with the off-the-shelf SG with respect to the quality of the deployed state. As proposed in [22], the following geometrical and mechanical parameters are used to assess the quality of the deployed state:

1. **Graft-vessel gap:** The graft-vessel gap g_n defines the distance between the outer surface of the SG and the luminal vessel surface (Figure 4I). Large graft-vessel gaps indicate an inappropriate attachment of the SG in the landing zones and increase the risk of endoleaks type I [17,6]. Further, large graft-vessel gaps might induce blood flow disturbances [45,7,27] which might contribute to intraprosthetic thrombotic deposits [59].

2. **Graft-vessel seal:** To properly seal the aneurysm leak-proof a good attachment of the SG to the luminal vessel surface is required. For points of the graft with a graft-vessel gap $g_n = 0$, i.e. SG and vessel are in contact, "seal" between SG and vessel is assumed. For all other points of the graft with $g_n > 0$ "no seal" is given (Figure 4I). The graft-vessel seal assesses the sealing pattern of the deployed SG and hence gives an indication of the likelihood of endoleaks type I [17,6]. It is important to note, that whether graft-vessel gaps lead to an endoleak type I or not strongly depends on the sealing pattern of the deployed SG, among other factors. As long as a complete circumferential seal of sufficient length is given in the landing of the SG, large graft-vessel gaps do not necessarily lead to an endoleak.

3. **Normal contact traction:** Normal contact tractions t_n in combination with friction between SG and vessel are responsible for the passive fixation of the SG in the vessel. However, local hot spots with excessive normal contact traction might also trigger local tissue remodeling or even might lead to erosion of the vessel wall [29,18].

4. **Stent stress:** The Cauchy von Mises equivalent stress measure is used to assess the stress state in the stent. Large stent stresses are associated with a higher risk of SG fatigue [24,3].

5. **SG fixation force:** In order to resist the pulsatile blood flow as well as blood pressure and prevent the SG from migrating [54,50,1], SGs are designed with an oversize with respect to the vessel diameter (equation (1)). The resulting contact tractions lead to a passive fixation force $\hat{F}$ of the SG [20]

$$\hat{F} = \int ||\mathbf{t}_n|| \, da \tag{5}$$

where $\mathbf{t}_n$ is the normal contact traction at the contact interface between SG and vessel. The integration area a corresponds to the total abluminal graft surface of the considered SG models in the deployed configuration. This force is named *passive* fixation force to clearly distinguish between the *active* SG fixation by barbs that is used by many marketed SGs.

These mechanical and geometrical parameters may give indications of potential EVAR related complications. However, the respective EVAR related complication and its consequences are not modeled. For instance, modeling of an endoleak type I would require modeling of blood flow. Further, the proposed parameters assess the EVAR outcome from a purely engineering perspective. Medical, biological or other parameters that also may have an influence on the occurrence of EVAR related complications are not evaluated. The incorporation of these parameters into a setting to be used in clinical practice is future work and beyond the scope of this contribution.
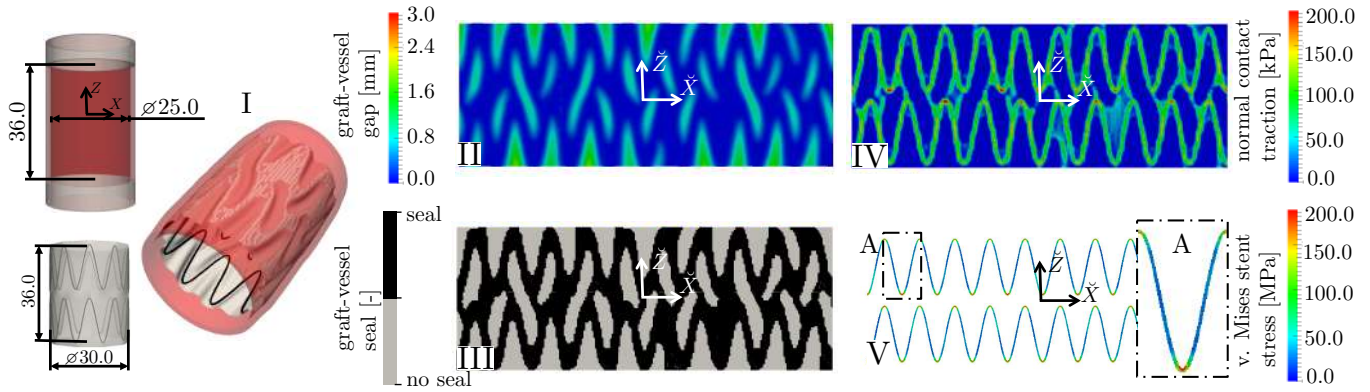
FIGURE 5 In silico EVAR results of a straight, cylindrical SG deployed in a straight, cylindrical vessel: deployed state (I), graft-vessel gap (II), graft-vessel seal (III), normal contact tractions between SG and vessel (IV) and Cauchy von Mises stent stresses (V).

3 | RESULTS

In the following we evaluate the deployed state of the off-the-shelf SG and the customized SG for all eight vessel morphologies with respect to the graft-vessel gap, the graft-vessel seal, the normal contact traction and the stent stresses in Figure 5-9 as well as with respect to the SG fixation force in Figure 10. For improved visualization of the results a projection of the results into the flat auxiliary $\check{X}\check{Z}$-plane is used in Figure 5-8. The auxiliary $\check{X}\check{Z}$-plane represents the uncoiled lateral surface of a virtual cylinder with radius $\check{R} = 15$ mm (Appendix B).

3.1 | Reference solution of straight, cylindrical vessel

As a reference, we first consider the in silico EVAR outcome in a straight, cylindrical vessel (Figure 5). A straight and cylindrical vessel is considered to be the optimal vessel morphology for the deployment of a SG[48,60]. For this setting, the off-the-shelf and the second level customized SG are identical.

A very uniform deployment and attachment of the cylindrical SG in the cylindrical vessel is obtained with moderate radial buckling of the graft (Figure 5I) due to 20% oversizing of the SG compared to the vessel. The SG is in direct contact with the vessel only at the location of the stent rings (Figure 5III). Minor radial buckling of the graft leads to a maximum gap between SG and vessel of approximately 1.5 mm (Figure 5II). A relatively uniform distribution of normal contact tractions of approximately 100 kPa is found between SG and vessel at the location of the stent rings (Figure 5IV). Maximum stent stresses of approximately 200 MPa occur in the curved parts of the stent rings (Figure 5V). The stress distribution is identical for each stent loop.

3.2 | Straight, conical vessel

The use of the cylindrical off-the-shelf SG with a constant diameter of 30 mm results in a degree of SG oversizing of 50% at the narrow end ($Z = 18$) of the conical vessel and a degree of SG oversizing of 0% at the wide end ($Z = -18$) of the conical vessel. In contrast to the off-the-shelf SG, the conical customized SG has a constant degree of SG oversizing of 20% along the total length of the SG (Figure 6).

A clear difference between the in silico EVAR outcome of the cylindrical off-the-shelf SG and the conical customized SG can be seen in Figure 6. A full expansion of the off-the-shelf SG at the wide end ($Z = -18$) and severe buckling of the graft at the narrow end ($Z = 18$), which results in larger graft-vessel gaps of up to 2.5 mm at the narrow end ($Z = 18$) can be identified. The off-the-shelf SG exerts high normal contact tractions at the narrow end. At the wide end ($Z = -18$) of the conical vessel, the off-the-shelf SG is not even in contact with the vessel. Unlike the off-the-shelf SG, the conical customized SG is more uniformly attached to the luminal vessel surface with a uniform distribution of normal contact tractions of approximately 100 kPa and very small gaps between SG and vessel. Due to the better and more uniform apposition of the SG to the vessel, the conical customized SG results in around 1.5 times higher SG fixation forces compared to the off-the-shelf SG in the same conical vessel (Figure 10).
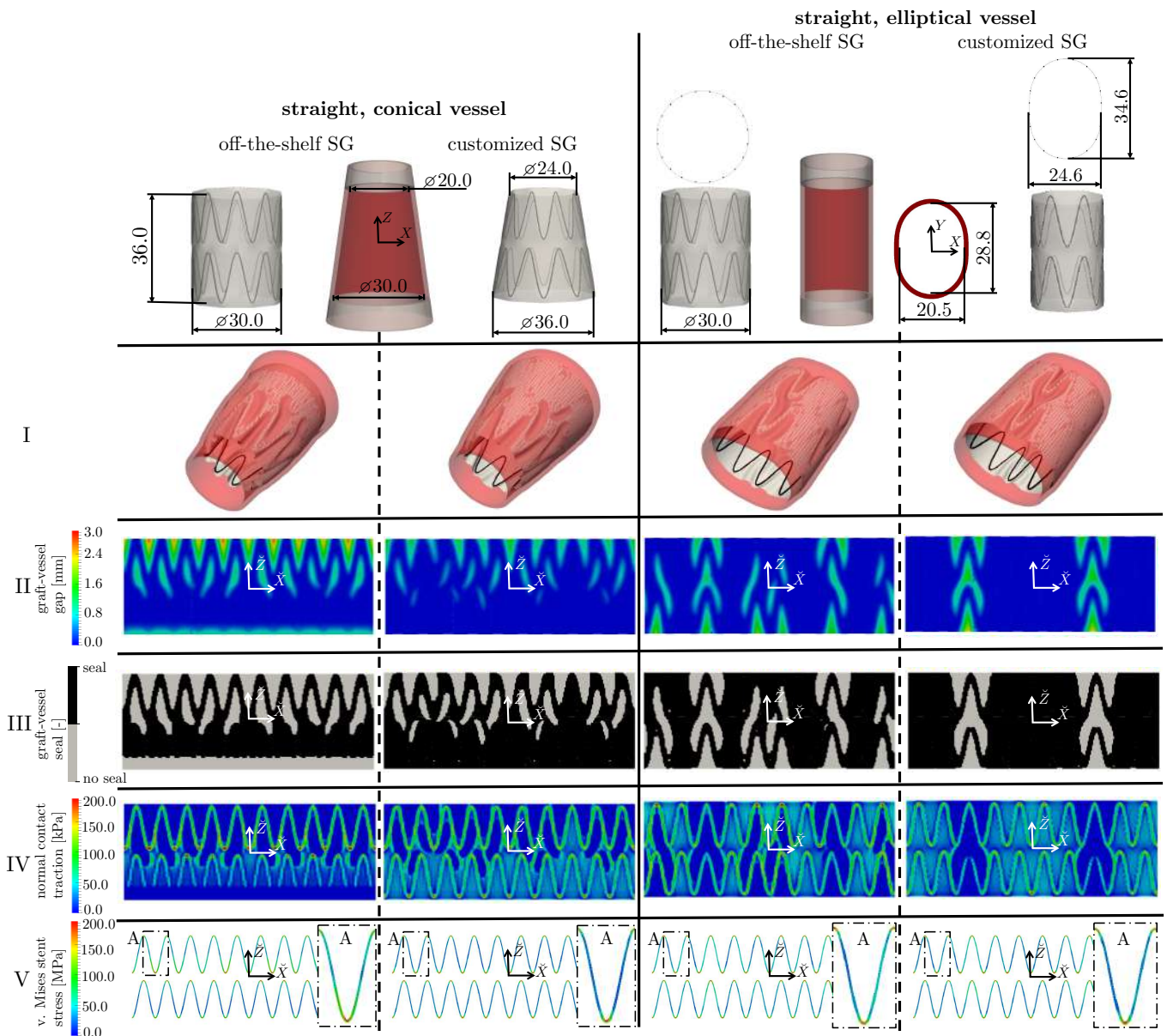
FIGURE 6 In silico EVAR results of off-the-shelf SGs and customized SGs deployed in a straight, conical vessel as well as in a straight, elliptical vessel: deployed state (I), graft-vessel gap (II), graft-vessel seal (III), normal contact tractions between SG and vessel (IV) and Cauchy von Mises stent stresses (V).

The deployed state of the customized SG in Figure 6I also shows that at the narrow end ($Z = -18$) more severe graft buckling is apparent than at the wide end ($Z = 18$), although constant SG oversizing of 20% is used along the total SG length. This shows that depending on the vessel diameter the same degree of SG oversizing can have a different influence on the deployed state.

3.3 | Straight, elliptical vessel

Only very minor differences between the deployed state of the off-the-shelf SG and the customized SG can be identified for the straight, elliptical vessel (Figure 6 and Figure 10). The graft-vessel sealing area is slightly larger for the customized SG since the off-the-shelf SG undergoes more graft buckling. The maximum graft-vessel gap, the distribution of stent stresses, the distribution of normal contact tractions as well as the SG fixation forces of the off-the-shelf SG and the customized SG are almost identical and very similar to the results obtained for the straight, cylindrical vessel (section 3.1).
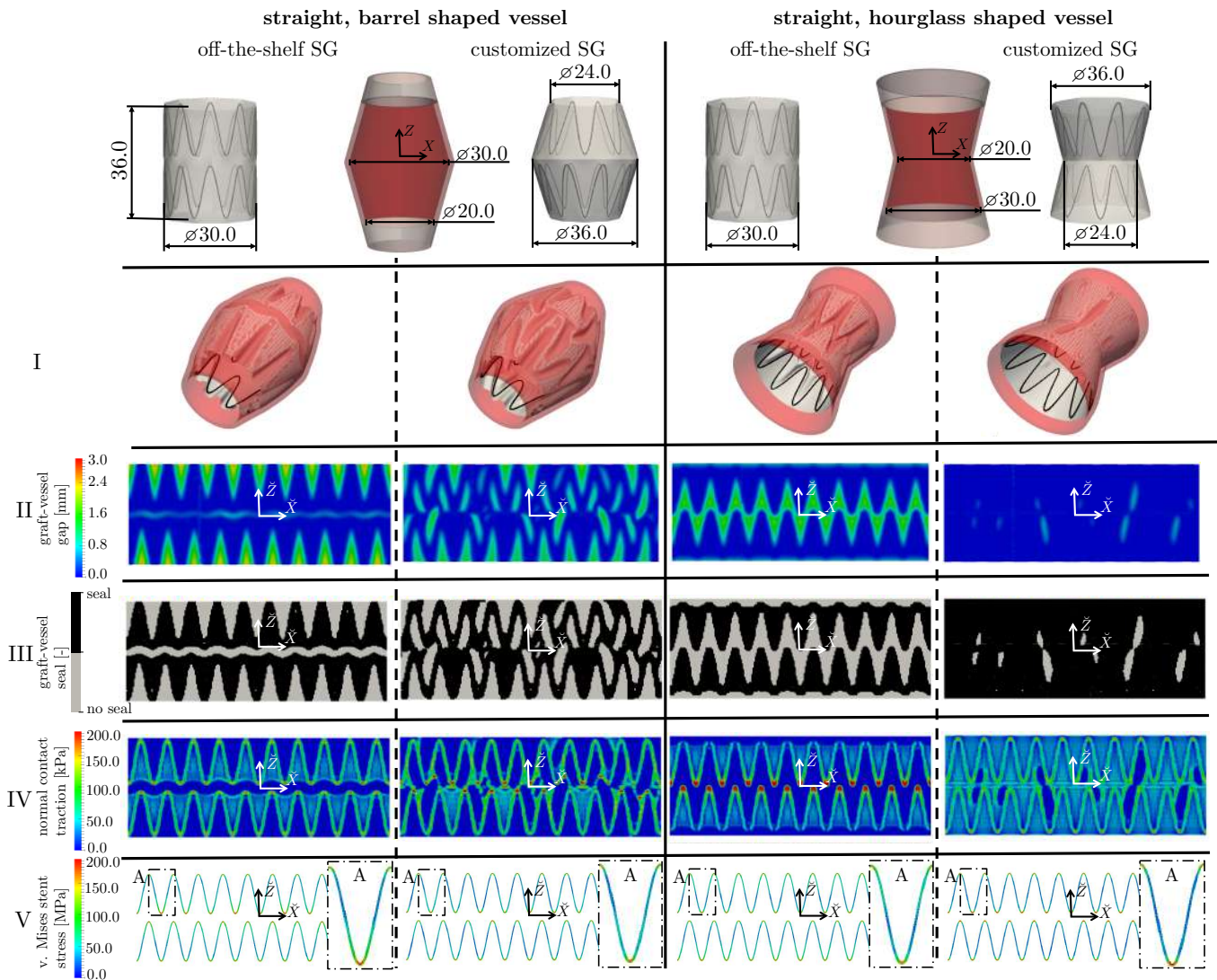
FIGURE 7 In silico EVAR results of off-the-shelf SGs and customized SGs deployed in a straight, barrel shaped vessel as well as in a straight, hourglass shaped vessel: deployed state (I), graft-vessel gap (II), graft-vessel seal (III), normal contact tractions between SG and vessel (IV) and Cauchy von Mises stent stresses (V).

3.4 | Straight, barrel shaped vessel

The deployed off-the-shelf SG has minimal graft buckling at the wide region of the vessel ($Z = 0$) and severe buckling at the narrow regions of the barrel shaped vessel, which leads to relatively large graft-vessel gaps of up to 2.8 mm (Figure 7). In contrast, the customized SG undergoes uniform graft buckling along the total SG and has a relatively uniform graft-vessel sealing pattern. The normal contact tractions between SG and vessel are slightly higher for the customized SG which results in approximately 1.2 times higher SG fixation forces (Figure 10). No discernible differences in stent stresses can be identified between the deployed off-the-shelf SG and the deployed customized SG.

3.5 | Straight, hourglass shaped vessel

The cylindrical off-the-shelf SG exhibits severe buckling of the graft with graft-vessel gaps of up to 2.0 mm whereas the customized SG almost fully expands and exhibits only minor buckling (Figure 7). The hourglass shaped customized SG in the hourglass shaped vessel leads to an almost complete seal between graft and vessel. The off-the-shelf SG produces high normal contact tractions between SG and vessel above 200 kPa at the narrow region of the vessel ($Z = 0$). Unlike the off-the-shelf
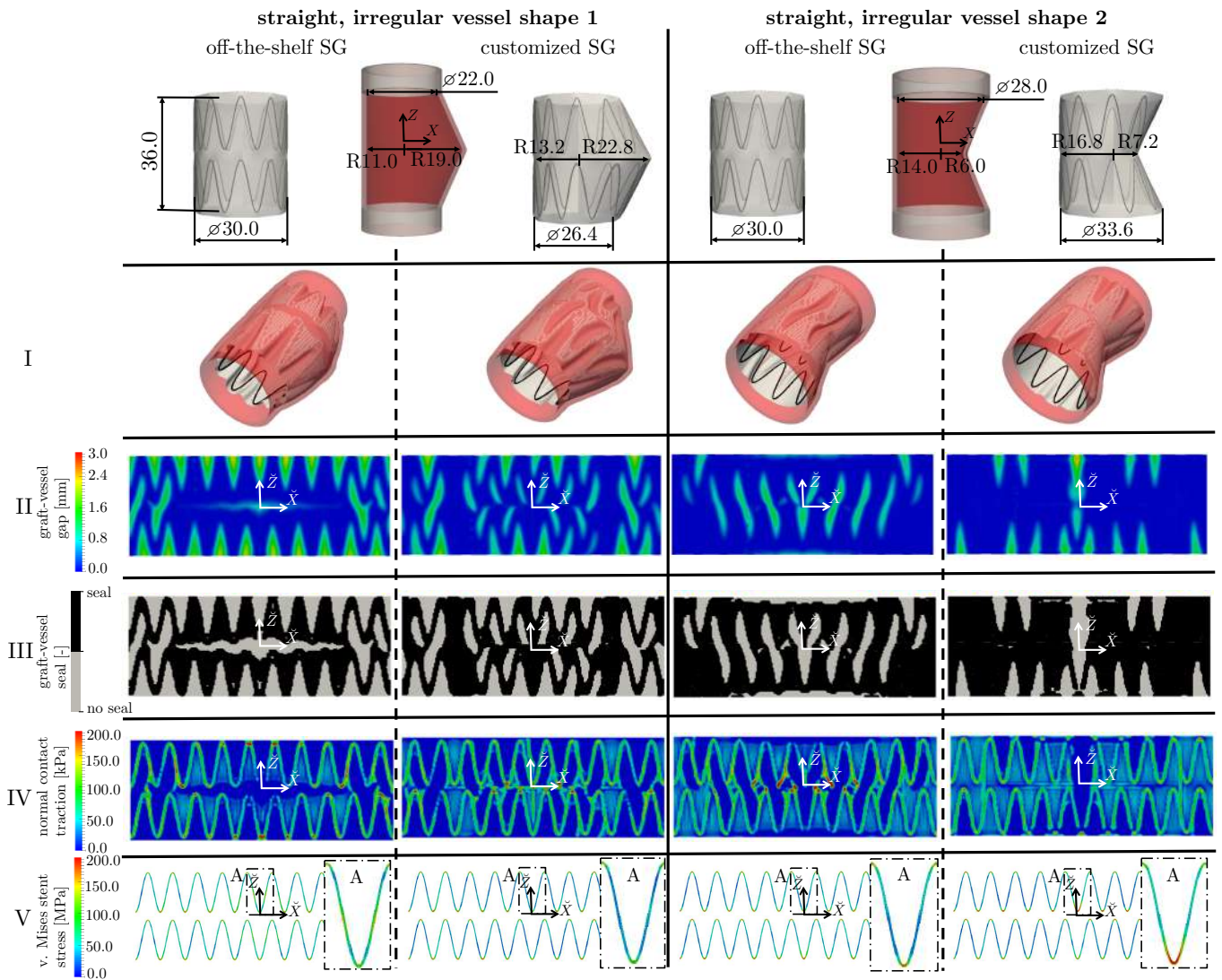
FIGURE 8 In silico EVAR results of off-the-shelf SGs and customized SGs deployed in two different straight, irregularly shaped vessels: deployed state (I), graft-vessel gap (II), graft-vessel seal (III), normal contact tractions between SG and vessel (IV) and Cauchy von Mises stent stresses (V).

SG, the distribution of normal contact tractions of the customized SG is very uniform without hotspots at the narrow region of the vessel ($Z = 0$). The stent stresses of the deployed customized SG are slightly higher than the stent stresses of the off-the-shelf SG (Figure 7). The use of the customized SG leads to approximately 1.5 times higher SG fixation forces compared to the off-the-shelf SG (Figure 10).

3.6 | Straight, irregular vessel shapes

In this section, the deployed SGs in two straight and irregularly shaped vessels are considered. The first vessel has a one-sided widening and the second vessel one-sided narrowing (Figure 8).

The results of the first irregular vessel are very similar to those from the straight, barrel shaped vessel (section 3.4) and the results of the second irregular vessel are very similar to the findings of the straight, hourglass shaped vessel (section 3.5). However, the difference between the off-the-shelf SG and the customized SG is less pronounced. While for the first irregular vessel model the customized SG results in slightly smaller stent stresses, for the second irregular vessel the customized SG results in slightly larger stent stresses in the highly curved parts of the stent rings.
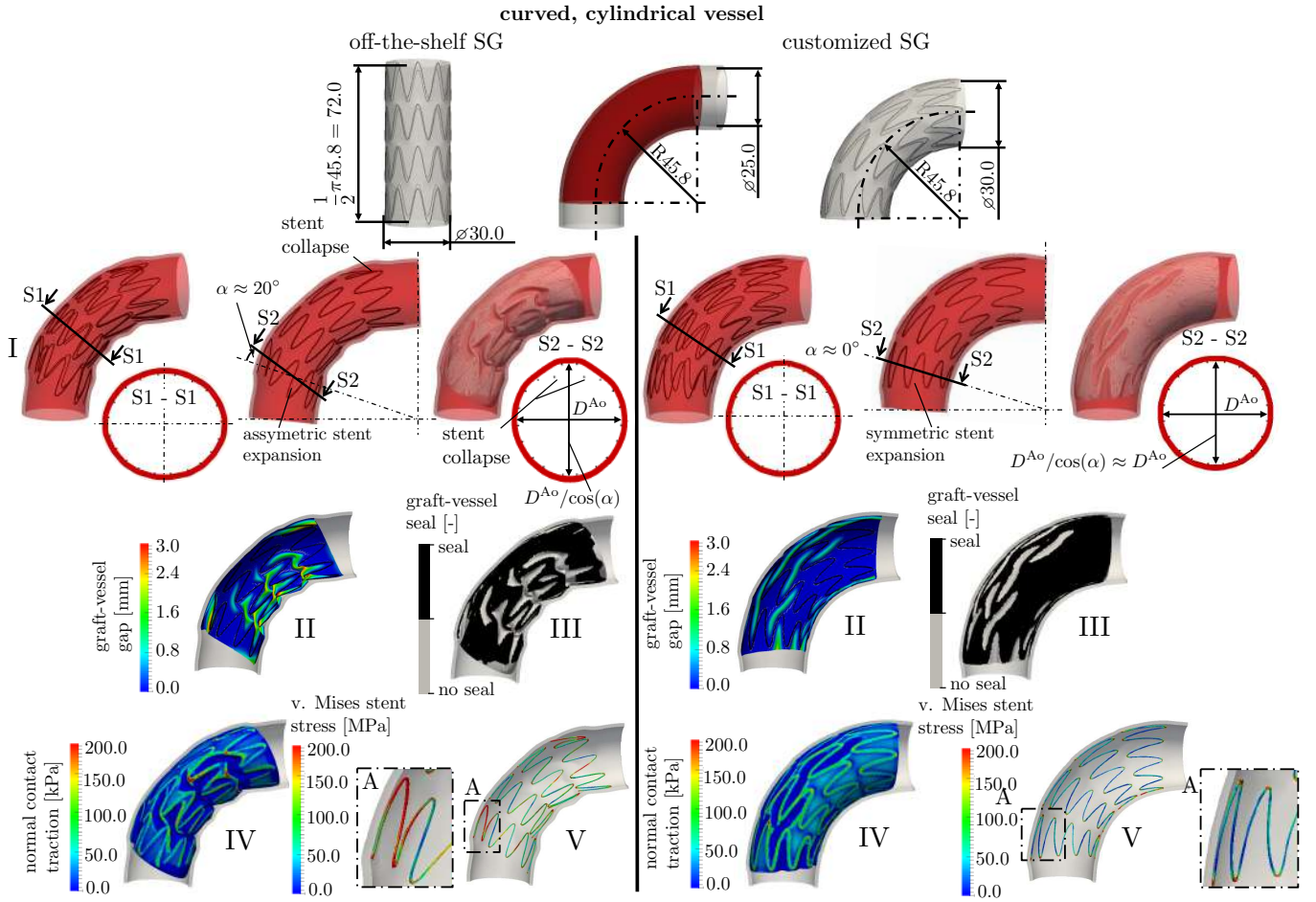
FIGURE 9 In silico EVAR results of an off-the-shelf SG and a customized SG deployed in a curved, cylindrical vessel: deployed state (I), graft-vessel gap (II), graft-vessel seal (III), normal contact tractions between SG and vessel (IV) and Cauchy von Mises stent stresses (V).

3.7 | Curved, cylindrical vessel

In the curved vessel (Figure 9), the straight off-the-shelf SG of length 72 mm is longer than the potential vessel landing zone at the inner curvature and shorter than the potential vessel landing zone at the outer curvature of the vessel by $2\Delta L = 19.6$ mm (equation (2)). Hence, the off-the-shelf SG is unable to adapt to the curved vessel, which results in severe longitudinal buckling of the graft at the inner curvature (Figure 9I) where the SG is longer than the corresponding vessel attachment side. In contrast to the off-the-shelf SG, the curved customized SG can almost perfectly adapt to the curved vessel. Only minor radial graft buckling exists and no stent collapse occurs.

The expansion of the first and last stent ring of the straight off-the-shelf SG is strongly asymmetric with an asymmetry angle α of approximately 20° (Figure 9I). The cross section of the vessel in a plane defined by the asymmetry angle α is elliptical (Figure 9I, slice S2). The circumference of the ellipse, i.e. the coverage length in circumferential direction, is larger than the circumference of a circular vessel cross section. Hence, asymmetric stent expansion results in a reduced degree of SG oversizing[53]. A purely geometric consideration of asymmetric stent expansion leads to the reduced degree of SG oversizing (cf. equation (1))

$$o_{\text{assym}} = \frac{D^{\text{SG}}}{\bar{D}^{\text{Ao}}_{\text{ellipse}}} - 1 = \frac{D^{\text{SG}}}{\sqrt{\frac{(D^{\text{Ao}})^2 + (D^{\text{Ao}}/\cos(\alpha))^2}{2}}} - 1 = \frac{D^{\text{SG}}}{D^{\text{Ao}}}\sqrt{\frac{2}{1 + 1/(\cos(\alpha))^2}} - 1 = (o+1)\sqrt{\frac{2}{1 + 1/(\cos(\alpha))^2}} - 1 \le o, \quad (6)$$

where $\bar{D}^{\text{Ao}}_{\text{ellipse}}$ is the quadratic mean diameter of the ellipse (equation (3)) that results from slicing the vessel in an angle of α with respect to the orthogonal plane to the vessel centerline (Figure 9I, slice S2). Further, in (6), D^{SG} is the undeformed SG diameter
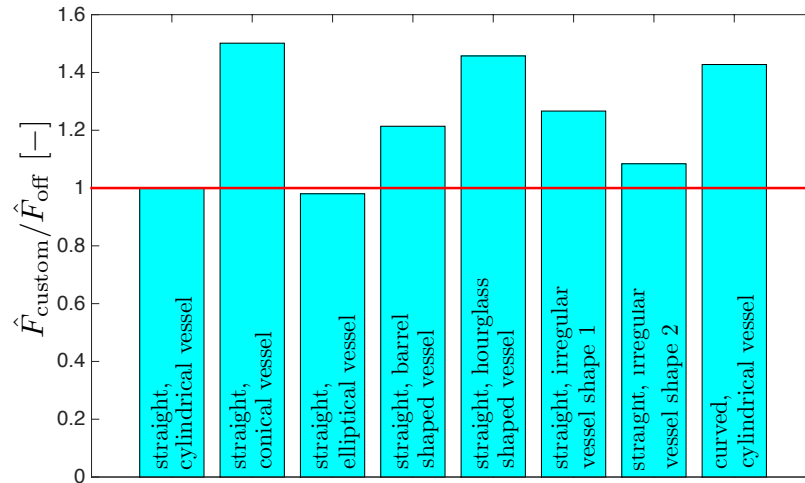
FIGURE 10 Relative difference of the SG fixation force (equation (5)) of customized SGs $\hat{F}_{\text{custom}}$ and off-the-shelf SGs $\hat{F}_{\text{off}}$ in the eight considered vessel morphologies. Values of $\hat{F}_{\text{custom}}/\hat{F}_{\text{off}} > 1$ illustrate the improvement of customized SGs with respect to the SG fixation force.

and D^{Ao} is the preinterventional vessel diameter. For the given asymmetric stent expansion of $\alpha \approx 20°$ of the off-the-shelf SG, the reduced degree of SG oversizing is $o_{\text{assym}} \approx 16.2\%$ compared to the nominal degree of SG oversizing of $o = 20\%$. Unlike the off-the-shelf SG, the customized SG does not lead to asymmetric stent expansion in the angulated vessel ($\alpha \approx 0°$, Figure 9I), i.e. $o_{\text{assym}} \approx o = 20\%$.

Stent collapse at the outer curve of the vessel at the first and last stent ring (Figure 9I, slice S2) with poor attachment between SG and vessel are further negative consequences of the deployment of the straight off-the-shelf SG in the angulated vessel.

Large gaps between SG and vessel above 3 mm exist at the inner curve of the vessel in the case of the off-the-shelf SG whereas the gaps between the customized SG and the curved vessel are below 1.5 mm (Figure 9II). At the critical inner curve of the vessel, the customized SG is almost fully in contact with the vessel (Figure 9III). Hence, in total the graft-vessel sealing is better in the case of the customized SG.

Due to the nonuniform compression of the straight off-the-shelf SG in the curved vessel, the stent rings are of elliptical shape in the deployed state with a major-to-minor axis ratio of 1.15 (Figure 9, slice S1). This results in higher normal contact tractions between SG and vessel at the major axis of the elliptical SG and lower normal contact tractions at the minor axis of the elliptical SG. The curved customized SG maintains its cylindrical shape even in the deployed state. Hence, the distribution of normal contact tractions is very uniform in the case of the customized SG (Figure 9IV).

The perfect attachment of the customized SG in the curved vessel as well as the uniform distribution of normal contact tractions is also reflected in around 1.5 times higher SG fixation forces compared to the off-the-shelf SG (Figure 10).

At the location of the collapsed stent parts of the off-the-shelf SG high stent stresses of above 500 MPa occur. In contrast, maximum stent stresses of approximately 300 MPa occur only at the curved parts of the stent rings of the customized SG (Figure 9V).

4 | DISCUSSION

In this study second level customized SGs with a morphology equivalent to the morphology of the luminal vessel surface were investigated. The comparison of the in silico EVAR outcome of straight, cylindrical off-the-shelf SGs and second level customized SGs has shown that using customized SGs can lead to considerably better EVAR outcomes. The numerical proof of concept of the benefit of customized SGs compared to off-the-shelf SGs was done with eight different vessel morphologies: seven straight vessels of different morphologies and one curved vessel with a circular cross section.

Noncylindrical vessel morphologies result in a variable degree of SG oversizing when cylindrical off-the-shelf SGs are used. For instance, in a conical vessel there is always the trade-off between SG undersizing, i.e. too little SG oversizing, at the wide end of the vessel and excessive SG oversizing at the narrow end of the vessel. This means there is always a trade-off between

complications associated with SG undersizing[54,52], such as SG migration and endoleaks, and complications related to excessive SG oversizing[9,47], such as postinterventional aortic neck dilatation. It was shown that by using second level customized SGs this inconsistency in choosing the degree of SG oversizing is obsolete. A constant degree of SG oversizing along the total length of the vessel landing zone could be achieved by using customized SGs that have the same morphology as the vessel.

Compared to the off-the-shelf SGs, the second level customized SGs led to reduced graft buckling and larger sealing areas. Furthermore, the maximum gaps between SG and vessel were smaller for customized SGs. In total, the improved appositioning of the customized SG to the vessel is a clear indicator that second level customized SGs might be able to reduce the likelihood of type I endoleaks in challenging aortic morphologies. Furthermore, the more uniform attachment of the customized SG to the vessel led to a more uniform distribution of normal contact tractions. Whilst off-the-shelf SGs partly led to local hot spots of normal contact tractions with increased risk of vessel damage or endograft infection[30,37], the distribution of normal contact tractions of customized SGs mostly was very uniform even in nonuniform vessel geometries. Using the same degree of SG oversizing, the customized SGs led to considerably larger passive fixation forces than the off-the-shelf SGs for all investigated vessel morphologies. Even if the likelihood of stent-graft migration is reduced by introduction of barbs in latest generation stent-graft devices[4], customization might further contribute positively to long-term fixation of the stent-graft without migration. Further, smaller degree of SG oversizing could be used for customized SGs to obtain the same passive fixation forces between SG and vessel and hence reduce potential negative effects of large SG oversizing[54,9,47].

The smallest impact of SG customization was identified for straight and elliptical vessels. It is explained by the relatively small lateral stiffness of a cylindrical SG. This means that little deformation energy is required to deform the cylindrical SG into an elliptical one. Hence, the mechanical behavior of the cylindrical off-the-shelf SG and the elliptical customized SG are almost identical.

The largest benefit of the customized SG compared to the off-the-shelf prosthesis could be observed for curved vessels as well as straight, conical vessels and straight, hourglass shaped vessels which are frequently observed vessel morphologies in clinical practice[31]. Using the customized SG in a curved vessel with an angle of 90° increased the passive SG fixation force by approximately 50%. This substantial difference in passive SG fixation force between the straight off-the-shelf SG and the curved customized SG can be explained by the following:

1. **The exploitation of the restricted length of the vessel landing zone is improved by second level customized SGs**, resulting in a considerably longer attachment length of the SG. A small SG attachment length is a frequently mentioned reason for insufficient SG fixation[61,1]. The effective length of the vessel landing zone is larger at the outer curvature than at the inner curvature of a curved vessel[53]. The straight off-the-shelf SG, whose length is sized according to the length of the vessel centerline, is too short to be able to fully exploit the effective length of the vessel landing zone at the outer curvature of an angulated vessel.

2. **Removal of longitudinal buckling at the inner curvature of angulated vessels by using second level customized SGs** which results in larger sealing areas and a more uniform radial force transmission between SG and vessel. The length of a straight off-the-shelf SG, which is sized according to the length of the vessel centerline, is longer than the effective length of the vessel landing zone at the inner curvature of the angulated vessel. This incompatibility between effective length of the vessel landing zone and the SG length leads to longitudinal compression of the graft at the inner curvature resulting in severe longitudinal buckling of the SG.

3. **Second level customized SGs do not show asymmetric stent expansion** which is associated with the reduction of the degree of SG oversizing[53]. The most proximal and the most distal stent rings of the investigated off-the-shelf SG showed asymmetric stent expansion with a reduction of the degree of SG oversizing from a nominal value of 20% to 16.2%. A smaller degree of SG oversizing is commonly associated with smaller radial forces between SG and vessel[10,20].

4. **No ovalization of second level customized SGs.** Bending of a straight off-the-shelf SG results in ovalization of the SG[12]. The SG with elliptic cross section does not fit perfectly into the vessel with circular cross section. It follows a nonuniform attachment between off-the-shelf SG and vessel with a nonuniform distribution of contact tractions.

5. **Second level customized SGs lead to a reduced risk of stent collapse.** The straight off-the-shelf SG lead to stent collapse located at the outer curvature of the vessel which is frequently observed for SGs in aortic necks with large angulation[23,5,1]. Stent collapse is associated with a loss of the SG-vessel attachment and hence a loss of radial force transmission between SG and vessel.

In addition to reduced SG-vessel attachment and reduced fixation forces, stent collapse of the off-the-shelf SG lead to locally high stent stresses within the region of the collapsed stent that might trigger SG fatigue[24,3]. Second level customized SGs did not show any stent collapse in the angulated vessel. Hence, maximum stent stresses and the likelihood of SG fatigue is reduced.

Besides reduced complication likelihoods, these positive results of second level customized SGs in vessels with large angulation are very promising to increase the range of applicability of EVAR far beyond the IFU of current SG manufacturers, i.e. far beyond the current restrictions to vessels with a neck angle below 60°.

5 | LIMITATIONS

Basic model simplifications were used in the in silico EVAR methodology. Instead of modeling the real-world medical intervention of EVAR, the in silico EVAR methodology only aimed at giving an approximation of the final deployed SG configuration. The pulsatile nature of blood flow was neglected. Instead, a quasi-static pressure state was considered. Dry friction using Coulomb's law was considered at the interface between SG and vessel. Lubrication between SG and vessel could not be considered by the purely solid mechanical model.

Further, in the presented examples we only considered the aortic neck whereas the aneurysm sac was not part of the model. Furthermore, improvements of the vessel model could be achieved by consideration of intraluminal thrombus and calcifications[28,20,21]. In the numerical proof of concept of this study only idealizations of realistic vessel shapes were considered. In future studies, the advantage of customized SGs in a realistic and patient-specific setting should be investigated.

Subject of this study was the investigation of the impact of the SG shape of customized SGs. Hence, the same material model was used for customized and off-the-shelf SGs. Slight differences in the material behavior of off-the-shelf SGs, that mostly use woven PET grafts, and the proposed customized electrospun grafts might have an impact on the outcome which should be investigated in further studies.

Finally, the SG morphology of the considered customized SGs was equivalent to the luminal vessel morphology. In clinical practice, accurate placement of SGs is facilitated by radiopaque markers and radiographic guidance, but precise placement of the SG remains very challenging. Hence, it is questionable if the morphology of the customized SG as an exact copy of the luminal vessel surface is the best choice taking into account the maximum SG placement accuracy. We assumed perfect placement of the SG, i.e. the shape of the customized SG fit perfectly to the luminal vessel surface. A sensitivity study of the effect of misplacement of customized SGs on the EVAR outcome should be investigated in future studies. Using a combination of topology and shape optimization, the performance of customized stent-grafts could be further improved. Topology optimization could be used to develop the patient-specific optimal design of the stent rings with respect to fixation forces and uniform attachment to the vessel. Shape optimization could be a valuable tool to determine the optimal morphology of the entire stent-graft for patient-specific cases. Such a topology and shape optimization of customized SGs should also consider the possible placement accuracy of the SG.

6 | CONCLUSIONS

Elevated EVAR related complication likelihoods are given in hostile aneurysm neck anatomies, where many of these complications are associated with a mismatch between SG and vessel. Highly customized SGs could considerably improve the quality of EVAR outcomes with reduced complication likelihoods and could increase the applicability of EVAR to patients with extreme vessel morphologies.

We presented models of highly customized SGs which have the same morphology as the luminal vessel surface. We numerically showed their advantage compared to off-the-shelf SGs in several different vessel morphologies. We compared the in silico EVAR outcome with respect to different mechanical and geometrical parameters such as stent stresses, contact tractions, SG fixation forces and the SG-vessel attachment. Especially SG fixation forces could be improved drastically by this type of SG customization leading to a better fixation of the deployed SG and potentially reduced likelihoods of SG migration.

In summary, this numerical proof of concept showed that the presented type of customized SGs can meet the demand of personalized therapy and can improve the EVAR outcome. The study motivates further development of highly personalized SGs towards the usage of customized SGs in clinical practice.

TABLE 1 Overview of constitutive models and material parameters of aortic wall and SG.

	Strain energy function	Material parameters			
Aortic wall [14,19]	$\Psi^{\mathrm{Ao}} = \dfrac{k_1}{2k_2}\displaystyle\sum_{i=4,6}(e^{k_2[\kappa\bar{I}_1+(1-3\kappa)\bar{I}_i-1]^2}-1)$ $+ c^{\mathrm{Ao}}(\bar{I}_1 - 3) + \Psi^{\mathrm{Ao}}_{\mathrm{vol}}(J)$	k_1 [kPa]	4070	k_2 [-]	165.6
		c^{Ao} [kPa]	100.9	κ [-]	0.16
		θ_i [°]	±48.4		
Stent [21,40,26]	$\Psi^{\mathrm{S}} = \dfrac{c^{\mathrm{S}}}{\beta^{\mathrm{S}}}(J^{-2\beta^{\mathrm{S}}} - 1) + c^{\mathrm{S}}(I_1 - 3)$	c^{S} [MPa]	6849	β^{S} [-]	5.75
Graft [20,46]	$\Psi^{\mathrm{G}} = \dfrac{c^{\mathrm{G}}}{\beta^{\mathrm{G}}}(J^{-2\beta^{\mathrm{G}}} - 1) + c^{\mathrm{G}}(I_1 - 3)$	c^{G} [MPa]	29.05	β^{G} [-]	2.625

7 | ACKNOWLEDGEMENTS

8 | CONFLICT OF INTEREST

All authors declare that no conflicts of interest exist.

APPENDIX A: CONSTITUTIVE MODELING

A overview of the vessel and SG constitutive models and model parameters is given in Table 1 where Ψ denotes the strain energy function (SEF) of the hyperelastic constitutive models, the superscript $(\bullet)^{\mathrm{Ao}}$ stands for the aortic wall, the superscript $(\bullet)^{\mathrm{S}}$ for the stent and the superscript $(\bullet)^{\mathrm{G}}$ for the graft.

I_1 is the first invariant of the right Cauchy-Green strain tensor and J is the determinant of the deformation gradient. $\bar{I}_1$ and $\bar{I}_2$ are the modified strain invariants of the right Cauchy-Green strain tensor. $\bar{I}_4$ and $\bar{I}_6$ are the squares of the stretches in mean fiber direction of the anisotropic two-fiber model with the transversely isotropic dispersion parameter κ. The mean fiber direction of the two fibers $i = \{4, 6\}$ in the local radial, axial and circumferential coordinate system of the aorta are given by $\mathbf{M}_i = [0, \sin(\theta_i), \cos(\theta_i)]^{\mathrm{T}}$. Ψ_{vol} is an Ogden type volumetric SEF[13,35] whose volumetric bulk modulus is chosen sufficiently large to sustain almost incompressibility of the aortic wall.

APPENDIX B: AUXILIARY PLANE FOR VISUALIZATION OF THE RESULTS

The coordinates of the flat auxiliary $\check{X}\check{Z}$-plane ($\check{Y} = 0$) are given by

$$\check{X} = \begin{cases} \check{R}\left(\arctan\left(\frac{Y}{X}\right) + \frac{\pi}{2}\right), & Y \leq 0 \\ \check{R}\left(\arctan\left(\frac{Y}{X}\right) - \frac{\pi}{2}\right), & Y > 0 \end{cases} \tag{7}$$

$$\check{Z} = Z \tag{8}$$

where X and Y are the reference coordinates of the SG and $\check{R}$ is the radius of a virtual cylinder.

References

1. H.-E. Altnji, B. Bou-Saïd, and H. Walter-Le Berre, Morphological and stent design risk factors to prevent migration phenomena for a thoracic aneurysm: a numerical analysis, *Medical engineering and physics* **37**, 23–33, 2015.

2. F. Auricchio, M. Conti, S. Marconi, A. Reali, J. L. Tolenaar, and S. Trimarchi, Patient-specific aortic endografting simulation: From diagnosis to prediction, *Computers in Biology and Medicine* **43**, 386 – 394, 2013.

3. H. G. Beebe, J. L. Cronenwett, B. T. Katzen, D. C. Brewster, R. M. Green, V. E. T. Investigators, et al., Results of an aortic endograft trial: impact of device failure beyond 12 months, *Journal of vascular surgery* **33**, 55–63, 2001.

4. J. Brunkwall, How to design the optimal stent graft—what have we learnt?, *Scandinavian Journal of Surgery* **97**, 191–194, 2008.

5. L. Canaud, P. Alric, M. Laurent, T.-P. Baum, P. Branchereau, C. H. Marty-Ané, and J.-P. Berthet, Proximal fixation of thoracic stent-grafts as a function of oversizing and increasing aortic arch angulation in human cadaveric aortas, *Journal of Endovascular Therapy* **15**, 326–334, 2008.

6. R. W. Chang, P. Goodney, L.-Y. Tucker, S. Okuhn, H. Hua, A. Rhoades, N. Sivamurthy, and B. Hill, Ten-year results of endovascular abdominal aortic aneurysm repair from a large multicenter registry, *Journal of vascular surgery* **58**, 324–332, 2013.

7. C. K. Chong and T. V. How, Flow patterns in an endovascular stent-graft for abdominal aortic aneurysm repair, *Journal of biomechanics* **37**, 89–97, 2004.

8. *Endovascular Aortic Repair - Abdominal.* Cook Medical, Bloomington, Indiana, USA, 2018.

9. T. Corbett, D. Molony, E. Kavanagh, P. Grace, M. Walsh, and T. McGloughlin, Experimental analysis of endovascular treatment of aaa and predictors of long term outcomes, *Biomechanics and Mechanobiology of Aneurysms*, 247–284, 2011.

10. S. De Bock, F. Iannaccone, M. De Beule, D. Van Loo, F. Vermassen, B. Verhegghe, and P. Segers, Filling the void: A coalescent numerical and experimental technique to determine aortic stent graft mechanics, *Journal of biomechanics* **46**, 2477–2482, 2013.

11. E. de Souza Neto, D. Perić, M. Dutko, and D. Owen, Design of simple low order finite elements for large strain analysis of nearly incompressible solids, *International Journal of Solids and Structures* **33**, 3277–3296, 1996.

12. N. Demanget, S. Avril, P. Badel, L. Orgéas, C. Geindreau, J.-N. Albertini, and J.-P. Favre, Computational comparison of the bending behavior of aortic stent-grafts, *Journal of the mechanical behavior of biomedical materials* **5**, 272–282, 2012.

13. S. Doll and K. Schweizerhof, On the development of volumetric strain energy functions, *Journal of applied mechanics* **67**, 17–21, 2000.

14. T. C. Gasser, R. W. Ogden, and G. A. Holzapfel, Hyperelastic modelling of arterial layers with distributed collagen fibre orientations, *Journal of the royal society interface* **3**, 15–35, 2006.

15. M. W. Gee, C. Förster, and W. A. Wall, A computational strategy for prestressing patient-specific biomechanical problems under finite deformation, *International Journal for Numerical Methods in Biomedical Engineering* **26**, 52–72, 2010.

16. M. Gitterle, A. Popp, M. W. Gee, and W. A. Wall, Finite deformation frictional mortar contact using a semi-smooth newton method with consistent linearization, *International Journal for Numerical Methods in Engineering* **84**, 543–571, 2010.

17. R. M. Greenhalgh and J. T. Powell, Endovascular repair of abdominal aortic aneurysm, *New England Journal of Medicine* **358**, 494–501, 2008.

18. K. A. Hance, J. Hsu, T. Eskew, and A. S. Hermreck, Secondary aortoesophageal fistula after endoluminal exclusion because of thoracic aortic transection, *Journal of vascular surgery* **37**, 886–888, 2003.

19. D. Haskett, G. Johnson, A. Zhou, U. Utzinger, and J. V. Geest, Microstructural and biomechanical alterations of the human aorta as a function of age and location, *Biomechanics and modeling in mechanobiology* **9**, 725–736, 2010.

20. A. Hemmler, B. Lutz, C. Reeps, G. Kalender, and M. W. Gee, A methodology for in silico endovascular repair of abdominal aortic aneurysms, *Biomechanics and Modeling in Mechanobiology* **17**, 1139–1164, 2018.

21. A. Hemmler, B. Lutz, G. Kalender, C. Reeps, and M. W. Gee, Patient-specific in silico endovascular repair of abdominal aortic aneurysms: application and validation, *Biomechanics and Modeling in Mechanobiology* **18**, 983–1004, 2019.

22. A. Hemmler, B. Lutz, C. Reeps, and M. W. Gee, In silico study of vessel and stent-graft parameters on the potential success of endovascular aneurysm repair, *International Journal for Numerical Methods in Biomedical Engineering* **online ahead of print**, https://doi.org/10.1002/cnm.3237, 2019.

23. M. M. Idu, J. A. Reekers, R. Balm, K.-J. Ponsen, B. A. de Mol, and D. A. Legemate, Collapse of a stent-graft following treatment of a traumatic thoracic aortic rupture, *Journal of Endovascular Therapy* **12**, 503–507, 2005.

24. T. S. Jacobs, J. Won, E. C. Gravereaux, P. L. Faries, N. Morrissey, V. J. Teodorescu, L. H. Hollier, and M. L. Marin, Mechanical failure of prosthetic human implants: a 10-year experience with aortic stent graft devices, *Journal of vascular surgery* **37**, 16–26, 2003.

25. W. D. Jordan, K. Ouriel, M. Mehta, D. Varnagy, W. M. Moore, F. R. Arko, J. Joye, J.-P. P. de Vries, J. P. de Vries, H. Eckstein, et al., Outcome-based anatomic criteria for defining the hostile aortic neck, *Journal of vascular surgery* **61**, 1383–1390, 2015.

26. C. Kleinstreuer, Z. Li, C. Basciano, S. Seelecke, and M. Farber, Computational mechanics of nitinol stent grafts, *Journal of biomechanics* **41**, 2370–2378, 2008.

27. Z. Li and C. Kleinstreuer, Blood flow and structure interactions in a stented abdominal aortic aneurysm model, *Medical engineering & physics* **27**, 369–382, 2005.

28. A. Maier, M. W. Gee, C. Reeps, H.-H. Eckstein, and W. A. Wall, Impact of calcifications on patient-specific wall stress analysis of abdominal aortic aneurysms, *Biomechanics and modeling in mechanobiology* **9**, 511–521, 2010.

29. R. Makar, J. Reid, A. Pherwani, L. Johnston, R. Hannon, B. Lee, and C. Soong, Aorto-enteric fistula following endovascular repair of abdominal aortic aneurysm, *European Journal of Vascular and Endovascular Surgery* **20**, 588–590, 2000.

30. G. Maleux, M. Koolen, and S. Heye, Complications after endovascular aneurysm repair, *Seminars in interventional radiology* **26**, 3–9, 2009.

31. C. O. McDonnell, M. Halak, A. Bartlett, and S. R. Baker, Abdominal aortic aneurysm neck morphology: proposed classification system, *Irish journal of medical science* **175**, 4–8, 2006.

32. I. V. Mohan, R. J. F. Laheij, and P. L. Harris, Risk factors for endoleak and the evidence for stent-graft oversizing in patients undergoing endovascular aneurysm repair, *European Journal of Vascular and Endovascular Surgery* **21**, 344–349, 2001.

33. P. Moireau, N. Xiao, M. Astorino, C. A. Figueroa, D. Chapelle, C. A. Taylor, and J.-F. Gerbeau, External tissue support and fluid–structure simulation in blood flows, *Biomechanics and modeling in mechanobiology* **11**, 1–18, 2012.

34. F. L. Moll, J. Powell, G. Fraedrich, F. Verzini, S. Haulon, M. Waltham, J. Van Herwaarden, P. Holt, J. Van Keulen, B. Rantner, et al., Management of abdominal aortic aneurysms clinical practice guidelines of the european society for vascular surgery, *European Journal of Vascular and Endovascular Surgery* **41**, S1–S58, 2011.

35. R. W. Ogden, Large deformation isotropic elasticity-on the correlation of theory and experiment for incompressible rubber-like solids, *Proceedings of the Royal Society of London A: Mathematical, Physical and Engineering Sciences (The Royal Society)* **326**, 565–584, 1972.

36. K. Oikonomou, R. Kopp, A. Katsargyris, K. Pfister, E. L. Verhoeven, and P. Kasprzak, Outcomes of fenestrated/branched endografting in post-dissection thoracoabdominal aortic aneurysms, *European Journal of Vascular and Endovascular Surgery* **48**, 641–648, 2014.

37. J. R. Parra, C. Lee, K. J. Hodgson, and B. Perler, Endograft infection leading to rupture of aortic aneurysm, *Journal of vascular surgery* **39**, 676–678, 2004.

38. S. W. Pattinson, M. E. Huber, S. Kim, J. Lee, S. Grunsfeld, R. Roberts, G. Dreifus, C. Meier, L. Liu, N. Hogan, et al., Additive manufacturing of biomechanically tailored meshes for compliant wearable and implantable devices, *Advanced Functional Materials* **online ahead of print**, doi.org/10.1002/adfm.201901815, 2019.

39. D. Perrin, P. Badel, L. Orgéas, C. Geindreau, A. Dumenil, J.-N. Albertini, and S. Avril, Patient-specific numerical simulation of stent-graft deployment: Validation on three clinical cases, *Journal of Biomechanics* **48**, 1868 – 1875, 2015.

40. D. Perrin, P. Badel, L. Orgeas, C. Geindreau, S. rolland du Roscoat, J.-N. Albertini, and S. Avril, Patient-specific simulation of endovascular repair surgery with tortuous aneurysms requiring flexible stent-grafts, *Journal of the Mechanical Behavior of Biomedical Materials* **63**, 86–99, 2016.

41. A. Popp, M. W. Gee, and W. A. Wall, A finite deformation mortar contact formulation using a primal–dual active set strategy, *International Journal for Numerical Methods in Engineering* **79**, 1354–1391, 2009.

42. C. Reeps, A. Maier, J. Pelisek, F. Härtl, V. Grabher-Meier, W. A. Wall, M. Essler, H.-H. Eckstein, and M. W. Gee, Measuring and modeling patient-specific distributions of material properties in abdominal aortic aneurysm wall, *Biomechanics and modeling in mechanobiology* **12**, 717–733, 2013.

43. K. A. Rocco, M. W. Maxfield, C. A. Best, E. W. Dean, and C. K. Breuer, In vivo applications of electrospun tissue-engineered vascular grafts: a review, *Tissue Engineering Part B: Reviews* **20**, 628–640, 2014.

44. R. M. Romarowski, M. Conti, S. Morganti, V. Grassi, M. Marrocco-Trischitta, S. Trimarchi, and F. Auricchio, Computational simulation of tevar in the ascending aorta for optimal endograft selection: A patient-specific case study, *Computers in biology and medicine* **103**, 140–147, 2018.

45. R. M. Romarowski, E. Faggiano, M. Conti, A. Reali, S. Morganti, and F. Auricchio, A novel computational framework to predict patient-specific hemodynamics after tevar: integration of structural and fluid-dynamics analysis by image elaboration, *Computers and Fluids* **179**, 806–819, 2019.

46. D. Roy, S. Lerouge, K. Inaekyan, C. Kauffmann, R. Mongrain, and G. Soulez, Experimental validation of more realistic computer models for stent-graft repair of abdominal aortic aneurysms, including pre-load assessment, *International journal for numerical methods in biomedical engineering* **32**, e02769, 2016.

47. S. M. Sampaio, J. M. Panneton, G. Mozes, J. C. Andrews, A. A. Noel, M. Kalra, T. C. Bower, K. J. Cherry, T. M. Sullivan, and P. Gloviczki, Aortic neck dilation after endovascular abdominal aortic aneurysm repair: should oversizing be blamed?, *Annals of vascular surgery* **20**, 338–345, 2006.

48. A. Schanzer, R. K. Greenberg, N. Hevelone, W. P. Robinson, M. H. Eslami, R. J. Goldberg, and L. Messina, Predictors of abdominal aortic aneurysm sac enlargement after endovascular repair, *Circulation* **123**, 2848–2855, 2011.

49. C. Singh, X. Wang, Y. Morsi, and C. S. Wong, Importance of stent-graft design for aortic arch aneurysm repair, *AIMS Bioengineering* **4**, 133, 2017.

50. W. C. Sternbergh, S. R. Money, R. K. Greenberg, T. A. Chuter, Z. Investigators, et al., Influence of endograft oversizing on device migration, endoleak, aneurysm shrinkage, and aortic neck dilation: results from the zenith multicenter trial, *Journal of vascular surgery* **39**, 20–26, 2004.

51. S. Vad, A. Eskinazi, T. Corbett, T. McGloughlin, and J. P. V. Geest, Determination of coefficient of friction for self-expanding stent-grafts, *Journal of biomechanical engineering* **132**, 121007, 2010.

52. T. J. van der Steenhoven, J. M. Heyligers, I. F. Tielliu, and C. J. Zeebregts, The upside down gore excluder contralateral leg without extracorporeal predeployment for aortic or iliac aneurysm exclusion, *Journal of vascular surgery* **53**, 1738–1741, 2011.

53. J. W. van Keulen, F. L. Moll, and J. A. van Herwaarden, Tips and techniques for optimal stent graft placement in angulated aneurysm necks, *Journal of vascular surgery* **52**, 1081–1086, 2010.

54. J. van Prehn, F. J. V. Schlösser, B. E. Muhs, H. J. M. Verhagen, F. L. Moll, and J. A. van Herwaarden, Oversizing of aortic stent grafts for abdominal aneurysm repair: a systematic review of the benefits and risks, *European Journal of Vascular and Endovascular Surgery* **38**, 42–53, 2009.

55. E. L. G. Verhoeven, G. Vourliotakis, W. T. G. J. Bos, I. F. J. Tielliu, C. J. Zeebregts, T. R. Prins, U. M. Bracale, and J. J. A. M. van den Dungen, Fenestrated stent grafting for short-necked and juxtarenal abdominal aortic aneurysm: an 8-year single-centre experience, *European Journal of Vascular and Endovascular Surgery* **39**, 529–536, 2010.

56. L. Vu-Quoc and X. G. Tan, Optimal solid shells for non-linear analyses of multilayer composites. i. statics, *Computer methods in applied mechanics and engineering* **192**, 975–1016, 2003.

57. E. Vukovic, M. Czerny, F. Beyersdorf, M. Wolkewitz, M. Berezowski, M. Siepe, P. Blanke, and B. Rylski, Abdominal aortic aneurysm neck remodeling after anaconda stent graft implantation, *Journal of vascular surgery* **68**, 1354–1359, 2018.

58. Y. G. Wolf, B. B. Hill, W. A. Lee, C. M. Corcoran, T. J. Fogarty, and C. K. Zarins, Eccentric stent graft compression: an indicator of insecure proximal fixation of aortic stent graft, *Journal of vascular surgery* **33**, 481–487, 2001.

59. I. H. Wu, P. C. Liang, S. C. Huang, N. S. Chi, F. Y. Lin, and S.-S. Wang, The significance of endograft geometry on the incidence of intraprosthetic thrombus deposits after abdominal endovascular grafting, *European Journal of Vascular and Endovascular Surgery* **38**, 741–747, 2009.

60. T. R. Wyss, F. Dick, L. C. Brown, and R. M. Greenhalgh, The influence of thrombus, calcification, angulation, and tortuosity of attachment sites on the time to the first graft-related complication after endovascular aneurysm repair, *Journal of vascular surgery* **54**, 965–971, 2011.

61. C. K. Zarins, D. A. Bloch, T. Crabtree, A. H. Matsumoto, R. A. White, and T. J. Fogarty, Stent graft migration after endovascular aneurysm repair: importance of proximal fixation, *Journal of vascular surgery* **38**, 1264–1272, 2003.

62. L. Zhang, X. Chen, and M. Liu, Research of customized aortic stent graft manufacture, In *IOP Conference Series: Materials Science and Engineering*, Volume 187, pages 1–9. IOP Publishing, 2017.